Vol. 6, No. 1, February 2022, pp. 44-50

Current Optics and Photonics

Regular Paper

Design and Fabrication of an Off-axis Elliptical Zone Plate in Visible Light

Nguyen Nu Hoang Anh[1,2], Hyug-Gyo Rhee[1,2]*, Pilseong Kang[2], and Young-Sik Ghim[1,2]**

[1]*Department of Science of Measurement, University of Science and Technology, Daejeon 34113, Korea*
[2]*Optical imaging and Metrology Team, Advanced Instrumentation Institute, Korea Research Institute of Standards and Science, Daejeon 34113, Korea*

(Received December 2, 2021 : revised January 6, 2022 : accepted January 10, 2022)

An off-axis zone plate is able to focus on a single order while neglecting the zeroth order in a visible imaging system. This allows one to enhance the contrast quality in diffractive images, which is the major advantage of this type of zone plate. However, most previous reflection zone plates are used in focusing X-rays with a small grazing incident angle and are intricately designed with the use of a local grating period. In this study, we suggest the design of an off-axis elliptical zone plate (EZP) that is used to focus a monochromatic light beam with separation between the first and unfocused orders under a large grazing incident angle of 45°. An assumption using the total grating period, which depends on the average and constant grating period, is proposed to calculate the desired distance between the first and zeroth order and to simplify the construction of a novel model off-center EZP. Four diffractive optical elements (DOEs) with different parameters were subsequently fabricated by direct laser lithography and then verified using a performance evaluation system to compare the results from the assumption with the experimental results.

Keywords : Diffractive optical elements, Laser lithography, Off-axis elliptical zone plate
OCIS codes : (090.0090) Holography; (090.1970) Diffractive optics; (220.3740) Lithography

I. INTRODUCTION

Visible light imaging has numerous applications in various fields in both science and daily life, such as quantitative imaging of human skin in microscopy [1], large-aperture telescopes [2], and digital devices [3–5]. In medicine in particular, imaging systems using visible light enable one to recover visual information, which contains more data than X-rays or ultrasound waves [6]. Therefore, visible light focusing has become an essential research topic in recent years.

An elliptical zone plate (EZP) [7–9] is widely used to focus visible light in organic light-emitting diodes (OLEDs) [10, 11] and liquid-crystal displays (LCDs) [12] when the incident beam and diffraction beam are not on the same axis. The purpose of such a plate is to maintain a circular zone plate shape [13], with the advantage of avoiding the light reflected from the plane and returning back to the light source. However, this type of zone plate causes all of the diffraction orders to be superposed, leading to contrast degradation of the image quality [14].

To address this issue, reflection zone plates [15–17], which consist of only part of the EZP far from the center, were developed and fabricated in previous studies. However, most prior models were used for X-ray focusing with a small grazing incident angle below 20° and depended on the distance between the source and the zone plate. Therefore, these types are not feasible for use with visible light

*Corresponding author: hrhee@kriss.re.kr, ORCID 0000-0003-3614-5909
**Corresponding author: young.ghim@kriss.re.kr, ORCID 0000-0002-4052-4939

Color versions of one or more of the figures in this paper are available online.

pISSN: 2508-7266 / eISSN: 2508-7274 https://doi.org/10.3807/COPP.2022.6.1.044

imaging systems, which require a relatively wide field of view. Moreover, the designs of these zone plates used the local grating period, which involves more complicated calculations and manufacturing processes.

In this study, an off-axis EZP, which is used to focus monochromatic light with a large grazing incident angle and that has the ability to divide the first order from the zeroth order, is proposed and fabricated by direct laser lithography given the advantages of this technique, *i.e.*, markless alignment and a flexible movement system [18–20]. This type of zone plate is able to be applied in imaging systems using a miniature target or laser plasma [21]. An assumption that relies on the total grating period, consisting of the average and constant period, for calculating the first-zeroth order distance is suggested. This design and assumption are experimentally verified on the focal plane using an optical evaluation system.

II. DESIGN OF REFLECTIVE ELLIPTICAL ZONE PLATE

Current EZPs are used to concentrate a parallel beam when the incident beam is not perpendicular to the surface of a zone plate. The structure of this zone plate is a sequence of elliptical gratings; it is expressed as [7]

$$\left(\frac{x}{a_n \cos\alpha}\right)^2 + \left(\frac{y - b_n}{a_n}\right)^2 = 1, \tag{1}$$

where $a_n = \sqrt{n\lambda\ f \quad + \frac{n\lambda}{}}$ / $\cos^2\alpha$ and $b_n = n\lambda$ sin α / 2 $\cos^2$ α.

The elliptical shape of the nth zone is centered at the origin with a width of $2a_n \cos\alpha$ and height of $2a_n$. As shown in Fig. 1, a beam source with a wavelength of λ is illuminated onto the EZP at incident angle α and concentrates the light at the distance of the focal length *f*, given by

$$f = \frac{a_1^2}{k\lambda\cos^2\alpha} - \frac{k\lambda}{4\cos^2\alpha}, \tag{2}$$

where a_1 is the half width of the first zone and *k* is the diffraction order. This demonstrates the influence of the focused order on the focal length, which leads to a decrease in the contrast in the diffractive image when the superposition outcome of all orders occurs [21]. This is the main weakness of prior EZP types. To deal with this issue, only an off-center quarter part of the EZP was used to focus an image. This new type of EZP was able to separate the first orders from the zeroth order spot, allowing the user to eliminate unfocused background noise from the diffractive image of the first order, which results in an enhancement of the contrast and thus an improvement in the image quality.

In this study, we investigated the design of the off-axis EZP with a desired distance from the first to the zeroth order. In Fig. 1, because the plane wave is not perpendicular to the grating normal to the central infinitesimal part of the EZP on the rectangular border, the regular grating equation could be used:

$$d(\cos\alpha - \cos\beta) = \lambda. \tag{3}$$

Here, *d* is the grating period, and β is the grazing diffraction angle at the first order. After using trigonometric formulas, the distance *h* between the first and the zeroth order was defined as

$$h = f \tan\left[\cos^{-1}\left(\cos\alpha - \frac{\lambda}{d}\right) - \alpha\right]. \tag{4}$$

Instead of computing the local grating period, which is complicated for an off-axis design, as in previous papers, we suggest a simple method by which the total grating period *d* that is applicable in visible light is calculated. Two types of grating periods and how they affect the total period

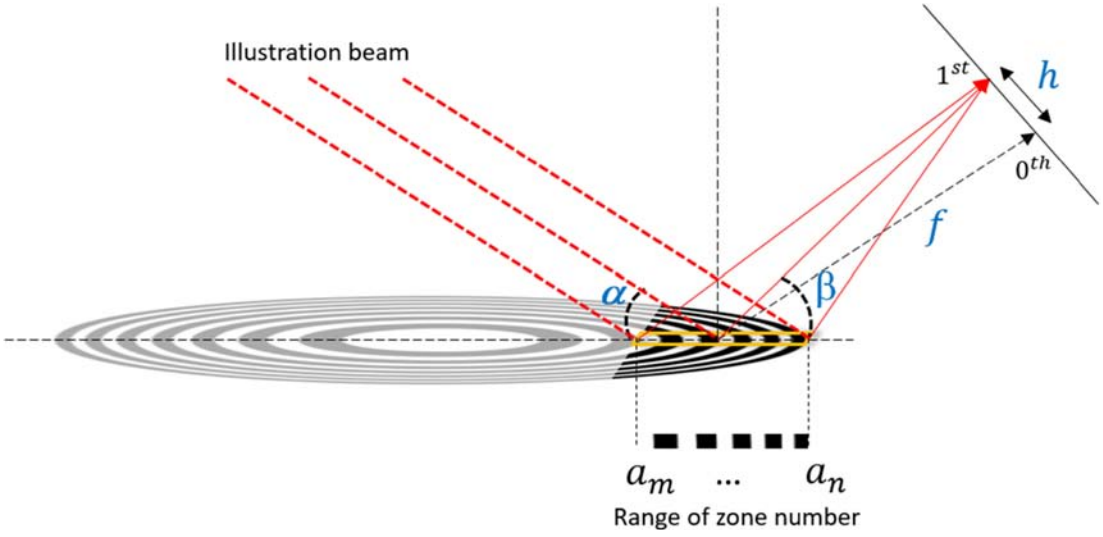

FIG. 1. Scheme of an off-axis elliptical zone plate (EZP) design.

are discussed.

The first is the average grating period. We consider a case with large number of zones, where the widths of the zones closest to the outermost areas are approximately equal. The average period grating in such a region is defined by

$$d_1 = \frac{a_n - a_m}{M}, \tag{5}$$

where d_1 is the average grating period and a_m and a_n are correspondingly the first zone and the outermost zone, and M is the number of slits.

The second type is referred to as the constant grating period [22]. When the EZP was small compared to the focal length, the semi-major axis of the EZP was approximated as $a_n = \sqrt{n\lambda f}\ /\ \cos\alpha$. Here, we proceed to convert the coordinate system of the original EZP from (x; y) to (a^2; α). As illustrated in Fig. 2(b), the transmission function of the EZP was similar to that of the traditional transmission grating, whose grating period was defined as

$$d_2 = 2a_1^2 \cos\alpha, \tag{6}$$

where d_2 is the constant grating period and a_1 is the semi-major height of the first zone. The total grating period depends on the average and constant periods; thus, an assumption pertaining to the total grating period of the off-axis EZP was brought forth:

$$d = Ad_1 + Bd_2. \tag{7}$$

Here, A and B are coefficients determined experimentally. The design parameters of the off-axis EZP consisted of the focal length f, grazing incident angle α, average grating period d_1 and constant grating period d_2. After defining these values, the design of the off-axis EZP with the desired distance between the first and zeroth order was created for a certain wavelength λ.

III. FABRICATION PROCESS

Direct laser lithography using a thermal chemical technique [23] was applied to manufacture the off-axis zone plate. This process included two main steps. First, the laser source with a wavelength of 488 nm was directly exposed to the chromium layer of the specimen that moved in a zigzag motion, as shown in Fig. 3(a). To avoid the ablation phenomenon, the distance between two adjacent points was adjusted in the range of 1.8 μm, as described in Fig. 3(b). The measurement results obtained by a commercial white-light scanning interferometer are shown in Figs. 3(c)–3(e). Finally, the specimen was dipped in an etchant solution of $K_3Fe(CN)_6$ and $NaOH$ to remove the remaining chromium and retain the part of the previously written pattern. To compare and verify this proposed assumption, four new off-axis EZPs, which were designed with the same grazing incident angle α = 45° and wavelength λ but with different focal lengths and ranges of zone numbers, were fabricated, as defined in Table 1.

IV. PERFORMANCE VERIFICATION

To evaluate the four proposed off-axis EZP with different focal lengths, a Basler charge-coupled device (CCD) camera with 659 × 494 pixels was put on a linear stage with a length of 200 mm, which allowed the CCD camera to move to the desired focal position, as presented in Fig. 4. At the zero position of the stage, there is an adjustable angle plate that keeps the EZP specimen at an angle of 45° in the direction of the incident light beam. A He-Ne laser head was used to emit the source beam with a wavelength of 632.8 nm and diameter of 1500 μm, and this beam went through a beam expander before being directed to whole surface of the off-axis EZP pattern. First, diffractive optical elements (DOE) 1 and 2 were placed on the adjustable angle plate, after which the CCD camera was pulled to the position of 80 mm on the linear stage to observe the diffractive image. Next, we replaced these specimens with DOE

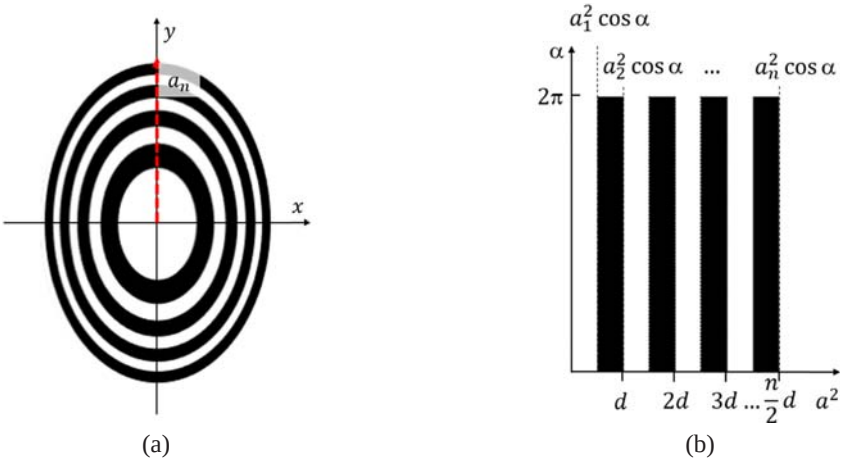

(a) (b)

FIG. 2. Transmission function of elliptical zone plate (EZP) in the (a) (x; y) and (b) (a^2; a) coordinate systems.

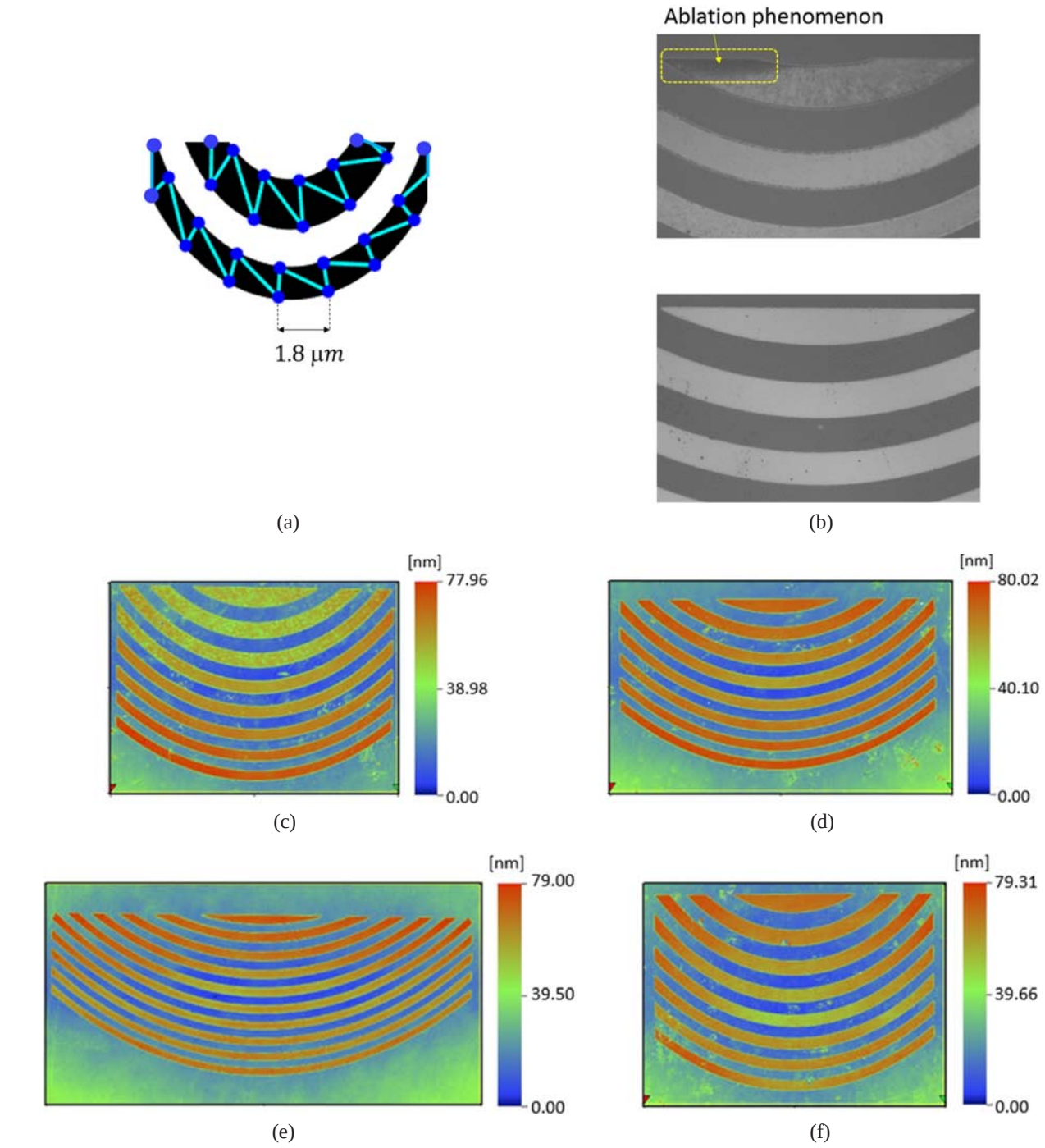

FIG. 3. Fabrication scheme and results: (a) specimen moved in a zigzag motion, (b) photographic view of an EZP, (c) measurement results of diffractive optical elements (DOE) 1, (d) DOE 2, (e) DOE 3, and (f) DOE 4.

TABLE 1. Design parameters of the four different diffractive optical elements (DOEs)

Type	Focal Length *f* (mm)	Range of Zone Number
DOE 1	80	5 to 20
DOE 2	80	9 to 24
DOE 3	80	21 to 40
DOE 4	120	5 to 20

3 and the distance from the object to the CCD camera was adjusted to 120 mm.

Figure 5 presents diffraction images of these off-axis EZPs. The first orders with full width half maximums of 49.5 μm, 39.6 μm, 29.7 μm, and 59.4 μm corresponding to DOE 1, DOE 2, DOE 3 and DOE 4, respectively, were separated from the background order. Moreover, the efficiency of these EZPs was approximately 6%, which was acceptable for an amplitude binary zone plate with mea-

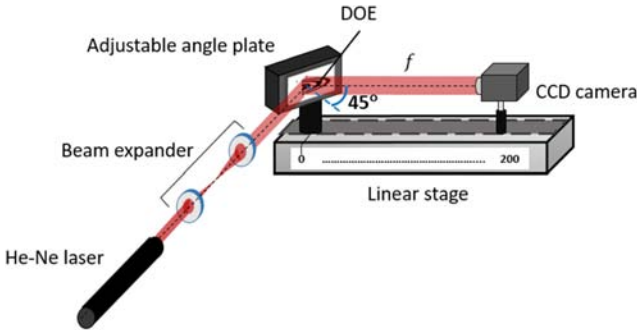

FIG. 4. Configuration of the experimental evaluation system.

sured efficiency from 1% to 10% [24]. It demonstrates the clear focusing ability of the newly designed off-axis EZP. The distance between the first and zeroth order of these EZPs is shown the experimental results, where four different equations with two variables are devised by adding all of the parameters to Eq. (4). After solving the pairs of equations, the coefficients *A* and *B*, which were well fitted to the four equations, were chosen, as defined in Table 2. Next, the percent difference between the experimental results and the calculation results was computed to be 2.7%. This indicates that the percentage difference between the two sets of results is small when the results are compared together.

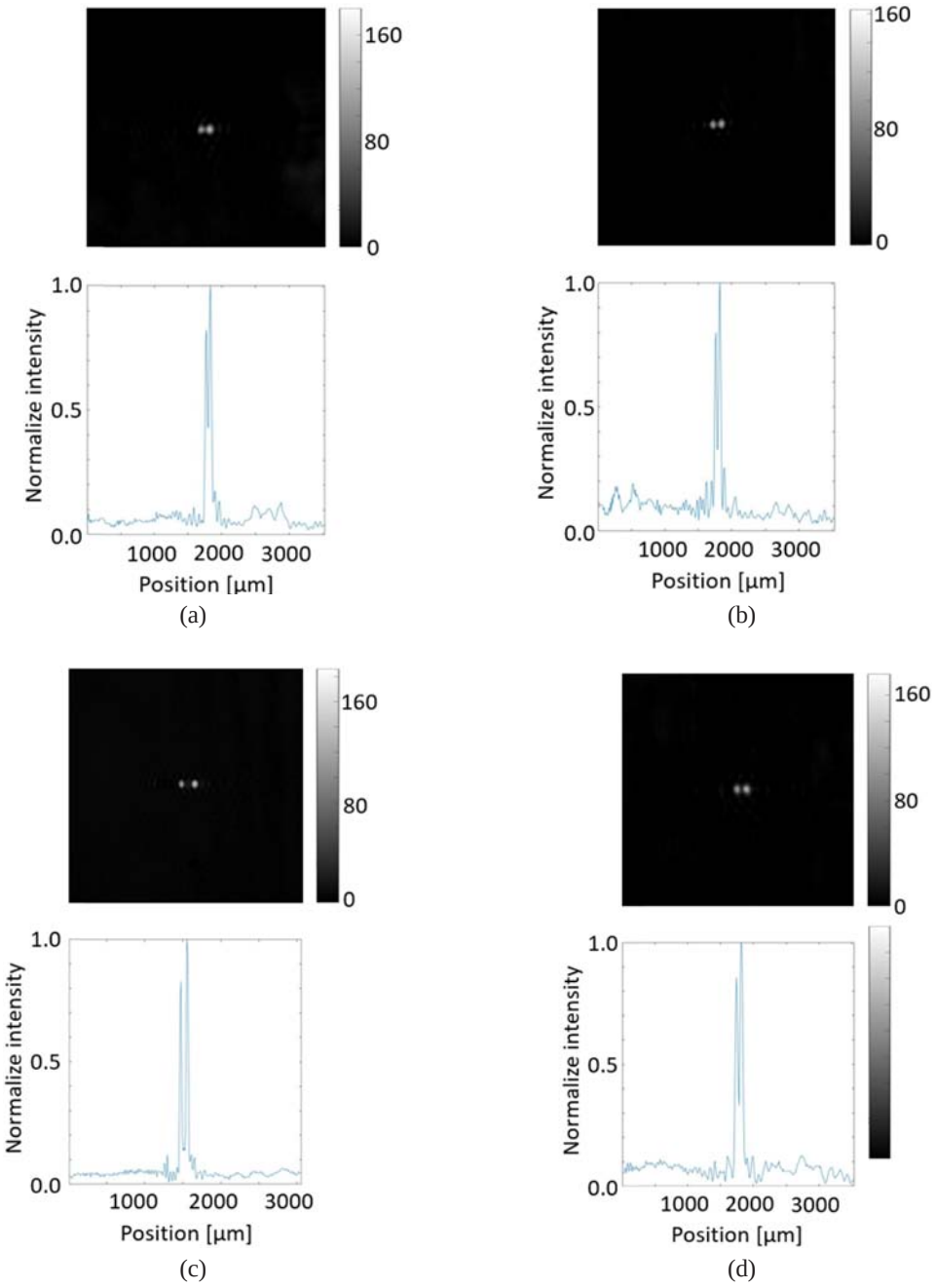

FIG. 5. Diffraction images of (a) diffractive optical element (DOE) 1, (b) DOE 2, (c) DOE 3 and (d) DOE 4.

TABLE 2. Results of the first-zeroth order distance of four diffractive optical elements (DOEs) and fitting coefficients

DOE 1	DOE 2	DOE 3	DOE 4	*A*	*B*	Percent Difference
$h = 58.7$ μm	$h = 72.5$ μm	$h = 128.7$ μm	$h = 79.0$ μm	16.792	−3.406	2.7%

Hence, the experimental results are in good agreement with the hypothetical results.

V. CONCLUSION

In this research, a quarter EZP was designed and fabricated by direct laser lithography. This proposed model is feasible for use with a visible imaging technique with a large grazing incident angle of 45° and can focus the first order beam without the overlap of the zeroth order one. This is the major advantage compared to previous EZP types. An assumption using the total grating period to calculate the distance between the first and unfocused order was demonstrated. In particular, the total grating period was found to depend on the average and constant period. Four EZPs with different focal lengths and off-center distances were verified using a performance evaluation system. The percent difference between the experimental results and the designed values was found to be small enough at less than 3%.

FUNDING

This study was supported by the Commercialization Promotion Agency for R&D Outcomes (COMPA), "Real-time 3D surface measurement for aspheric and freeform lens," funded by the Ministry of Science and ICT (MSIT).

REFERENCES

1. S. P. Chong, Z. Y. G. Ko, and N. Chen, "Visible light optical coherence microscopy for quantitative imaging of human skin in vivo," Proc. SPIE **11211**, 1121109 (2020).
2. Z. Xu, C. Yang, P. Zhang, X. Zhang, Z. Cao, Q. Mu, Q. Sun, and L. Xuan, "Visible light high-resolution imaging system for large aperture telescope by liquid crystal adaptive optics with phase diversity technique," Sci. Rep. **7**, 10034 (2017).
3. W. J. Mandl, "Visible light imaging sensor with A/D conversion at the pixel," Proc. SPIE **3649**, 2–13 (1999).
4. W. Zhao and K. Sakurai, "Seeing elements by visible-light digital camera," Sci. Rep. **7**, 45472 (2017).
5. Z. Li, Z. Zhang, Q. Yuan, Y. Qiao, K. Liao, and H. Yu, "Digital image processing in led visible light communications using mobile phone camera," in *Proc. 5th International Conference on Network Infrastructure and Digital Content-IEEE IC-NIDC* (Beijing, China, Sept. 2016), pp. 239–243.
6. G. Satat, B. Heshmat, D. Raviv, and R. Raskar, "All photons imaging through volumetric scattering," Sci. Rep. **6**, 33946 (2016).
7. Y. Wang, K. Kumar, L. Wang, and X. Zhang, "Monolithic integration of binary-phase Fresnel zone plate objectives on 2-axis scanning micromirrors for compact microendoscopes," Opt. Express **20**, 6657–6668 (2012).
8. N. N. H. Anh, Y.-G. Kim, H.-G. Rhee, and Y.-S. Ghim, "Novel fabrication process for an array of elliptical zone plates by using direct laser lithography," Int. J. Adv. Manuf. Technol. **106**, 2629–2634 (2020).
9. N. N. H. Anh, H.-G. Rhee, and Y.-S. Ghim, "Design and lithographic fabrication of elliptical zone plate array with high fill factor," Curr. Opt. Photonics **5**, 8–15 (2021).
10. K. Zhong, Y. Fu, and G. Jiang, "Improvement in light outcoupling efficiency of OLED by using high fill factor parabola curve microlens arrays," Optik **212**, 164604 (2020).
11. H. S. Kim, S. Il Moon, D. E. Hwang, K. W. Jeong, C. K. Kim, D.-G. Moon, and C. Hong, "Novel fabrication method of microlens arrays with high OLED outcoupling efficiency," Opt. Laser Technol. **77**, 104–110 (2016).
12. K. Huang, Y. Gan, Q. Wang, and X. Jiang, "Enhanced light extraction efficiency of integrated LEDs devices 7with the taper holes microstructures arrays," Opt. Laser Technol. **72**, 134–138 (2015).
13. H. Kim and S.-Y. Lee, "Optical phase properties of small numbers of nanoslits and an application for higher-efficiency fresnel zone plates," Curr. Opt. Photonics **3**, 285–291 (2019).
14. M. Grigoriev, R. Fakhrtdinov, D. Irzhak, A. Firsov, A. Firsov, A. Svintsov, A. Erko, and D. Roshchupkin, "Two-dimensional X-ray focusing by off-axis grazing incidence phase Fresnel zone plate on the laboratory X-ray source," Opt. Commun. **385**, 15–18 (2017).
15. M. Ibek, T. Leitner, A. Erko, A. Firsov, and P. Wernet, "Monochromatizing and focussing femtosecond high-order harmonic radiation with one optical element," Rev. Sci. Instrum. **84**, 103102 (2013).
16. M. Brzhezinskaya, A. Firsov, K. Holldack, T. Kachel, R. Mitzner, N. Pontius, J. S. Schmidt, M. Sperling, C. Stamm, A. Föhlisch, and A. Erko, "A novel monochromator for experiments with ultrashort X-ray pulses," J. Synchrotron Radiat. **20**, 522–530 (2013).
17. J. Metje, M. Borgwardt, A. Moguilevski, A. Kothe, N. Engel, M. Wilke, R. Al-Obaidi, D. Tolksdorf, A. Firsov, M. Brzhezinskaya, A. Erko, I. Y. Kiyan, and E. F. Aziz, "Monochromatization of femtosecond XUV light pulses with the use of reflection zone plates," Opt. Express **22**, 10747–10760 (2014).
18. Y.-G. Kim, H.-G. Rhee, Y.-S. Ghim, H.-S. Yang, and Y.-W. Lee, "Dual-line fabrication method in direct laser lithography to reduce the manufacturing time of diffractive optics elements," Opt. Express **25**, 1636–1645 (2017).
19. H.-G. Rhee and Y.-W. Lee, "Improvement of linewidth in laser beam lithographed computer generated hologram," Opt. Express **18**, 1734–1740 (2010).
20. Y.-G. Kim, H.-G. Rhee, Y.-S. Ghim, and Y.-W. Lee, "Method of fabricating an array of diffractive optical elements by using

a direct laser lithography," Int. J. Adv. Manuf. Technol. **101**, 1681–1685 (2019).
21. H. Merdji, G. Souillé, M. Idir, G. Cauchon, A. Mirone, C. Chenais-Popovics, and P. Dhez, "2-D X-ray laser-plasma imaging using Bragg Fresnel multilayer zone plates," Opt. Commun. **155**, 398–405 (1998).
22. Q. Fan, S. Wang, Z. Yang, L. Wei, F. Hu, H. Zang, Q. Zhang, C. Wang, G. Jiang, and L. Cao, "The realization of long focal depth with a linear varied-area zone plate," J. Mod. Opt. **64**, 244–250 (2017).
23. A. G. Poleshchuk, E. G. Churin, V. P. Koronkevich, V. P. Korolkov, A. A. Kharissov, V. V. Cherkashin, V. P. Kiryanov, A. V. Kiryanov, S. A. Kokarev, and A. G. Verhoglyad, "Polar coordinate laser pattern generator for fabrication of diffractive optical elements with arbitrary structure," Appl. Opt. **38**, 1295–1301 (1999).
24. S. Chen, A. Lyon, J. Kirz, S. Seshadri, Y. Feng, M. Feser, S. Sassolini, F. Duewer, X. Zeng, and C. Huang, "Absolute efficiency measurement of high-performance zone plates," Proc. SPIE **7448**, 74480D (2009).